Journal of Zhejiang University-SCIENCE A (Applied Physics & Engineering)
ISSN 1673-565X (Print); ISSN 1862-1775 (Online)
www.zju.edu.cn/jzus; www.springerlink.com
E-mail: jzus@zju.edu.cn

Numerical computations of the flow in a finite diverging channel*

Zhao-sheng YU†, Xue-ming SHAO, Jian-zhong LIN

(*State Key Laboratory of Fluid Power Transmission and Control, Department of Mechanics, Zhejiang University, Hangzhou 310027, China*)

†E-mail: yuzhaosheng@zju.edu.cn

Received Nov. 11, 2008; Revision accepted Mar. 6, 2009; Crosschecked Nov. 5, 2009

Abstract: The flow in a finite diverging channel opening into a large space and resembling the experimental prototype of Putkaradze and Vorobieff (2006) was numerically investigated. The effects of the Reynolds number, initial condition, intersection angle, length of the wedge edges, and the outer boundary condition were examined. The numerical results showed that the flow in the wedge undergoes a change from symmetrical flow to unsymmetrical flow with a weak backflow, then a vortical (circulation) flow and finally an unsteady jet flow as the Reynolds number is increased for an intersection angle of 32° and a wedge edge of length 30 times the width of the inlet slit. For the unsteady flow, the jet attached to one side of the wedge constantly loses stability and rolls up into a mushroom-shaped vortex-pair near the outlet of the wedge. As the intersection angle is increased to 50°, a stable jet flow is observed as a new regime between the vortex and unsteady regimes. Both the intersection angle and the wedge length have negative effects on the stability of the flow, although the effect of the wedge length on the critical Reynolds number for the symmetry-breaking instability is not pronounced. The outer boundary condition was found not to affect the flow patterns inside the wedge significantly. At a certain *Re* regime above the onset of symmetry-breaking instability, the flows evolve into steady state very slowly except for the initial stage in the case of decreasing flow flux. Two different solutions can be observed within the normal observation time for the experiment, providing a possible explanation for the hysteresis phenomenon in the experiment.

Key words: Diverging channel, Flow structures, Bifurcation, Fictitious domain
doi:10.1631/jzus.A0800782 **Document code:** A **CLC number:** O35

1 Introduction

The flow in a wedge-shaped channel is of great interest in fluid mechanics due to its simple geometry and practical applications to nozzles and diffusers (Schlichting and Gersten, 2000; Landau and Lifshitz, 1987). For the ideal case where the inlet and outlet effects are not considered, one could assume that the flow takes place only in the radial direction. Such a flow is called Jeffery-Hamel flow in the literature, for Jeffery (1915) and Hamel (1916) first derived the analytical solution. Fraenkel (1962) examined the various types of Jeffery-Hamel flow solutions, such as symmetrical unidirectional flow, symmetrical flow with backflow and unsymmetrical flow for the case of diverging flow. Hooper *et al.* (1982) discussed the effect of non-uniform viscosity on Jeffery-Hamel flow, and Stow *et al.* (2001) considered 3D extensions. There have been many studies on the analysis of the stability of the Jeffery-Hamel flow (Georgiou and Eagles, 1985; Sobey and Drazin, 1986; Allmen and Eagles, 1988; Eagles, 1988; Banks *et al.*, 1988; Hamadiche *et al.*, 1994; Uribe *et al.*, 1997; McAlpine and Drazin, 1998). The 2D flows in different expanding channels that are relevant to the Jeffery-Hamel flow have been investigated numerically (Sobey and Drazin, 1986; Goldshtik *et al.*, 1991; Tutty, 1996; Dennis *et al.*, 1997; Kerswell *et al.*, 2004) and experimentally (Sobey and Drazin, 1986; Nakayama, 1988; Putkaradze and Vorobieff, 2006). For example, Sobey and Drazin (1986) examined the flow in an indented channel numerically and experimentally. Tutty (1996) and Kerswell *et al.* (2004) numerically investigated the

* Project supported by the National Basic Research Program (973) of China (No. 2006CB705400), and the National Natural Science Foundation of China (Nos. 10602051 and 50735004)

steady nonlinear waves in a channel composed of a horizontal inlet part, a rapidly expanding part, a gradually expanding part and a horizontal outlet part. Dennis *et al.* (1997) considered a channel with an arc-shaped inlet and outlet. Majdalani and Zhou (2003) examined the incompressible laminar flow in a porous channel with expanding or contracting walls. Burde *et al.* (2007) investigated the stability of the flow in an expanding rotating porous cylinder. Boutros *et al.* (2007) solved the 2D viscous flow between slowly expanding or contracting walls with weak permeability using the Lie-group method. In contrast to other studies, Putkaradze and Vorobieff (2006) examined experimentally the flow in an expanding wedge that opened into a space much larger than the volume enclosed within the wedge. They observed a stable steady symmetrical flow at a relatively low Reynolds number and a steady unsymmetrical flow with a vortex (actually a circulation flow) occupying almost the entire inner space of the wedge at a higher Reynolds number. Interestingly, the critical Reynolds number for the transition from the symmetrical regime to the vortex regime by increasing the flow flux (Re_{ci}) was larger than the that of the reverse transition by decreasing the flow flux (Re_{cd}), a hysteresis phenomenon. For a Reynolds number between Re_{ci} and Re_{cd}, depending on whether the flow flux was increased or decreased, two different solutions were observed: one was an unsteady quasi-symmetrical flow for increasing flux and the other was a steady unsymmetrical flow for decreasing flux.

The aim of the present study was to gain a better understanding of the flow in a finite diverging channel resembling the experimental channel of Putkaradze and Vorobieff (2006) by a numerical simulation method. It should be emphasized that our flow model only resembles the experimental one and is not exactly the same. The experimental flow condition at the inlet cannot be reproduced exactly in our model owing to the fact that random disturbance to the inlet velocity is always present in an experiment and it is difficult to maintain the velocity (or flux) at the inlet for a long period of time, particularly with a diverging channel. In the present study, we considered only an idealized flow condition at the inlet: a given velocity profile that never changes with time. There may also exist other differences between our numerical model and the experimental prototype. Therefore, the numerical and experimental results cannot be used to validate each other and we did not aim to validate our code or to confirm or to refute the experimental observations in the present study, although we compared the two results whenever appropriate. We addressed the following issues:

1. The effect of the Reynolds number. Putkaradze and Vorobieff (2006) observed the transition from the symmetrical flow to the vortical (circulation) flow as *Re* increases. It is not clear what flow structures will occur when *Re* is further increased.

2. The effect of the initial condition. We examined whether the hysteresis phenomenon observed in the experiment would take place in our numerical flow model. Our results showed that at a certain *Re* regime above the onset of symmetry-breaking instability, the flows evolve into steady state very slowly except for the initial stage in the case of decreasing flow flux. Two different solutions can be observed within the normal observation time for the experiment, which provides a possible explanation for the hysteresis phenomenon in the experiment. We stress that, because of the differences between our model and the experimental prototype mentioned above, our simulations cannot predict what really took place in the experiment and therefore cannot exclude the possibility that there were other underlying physics for the hysteresis observed in the experiment.

3. The effect of the intersection angle of the wedge edges. We examined mainly whether the flow structures undergo similar transitions with increasing *Re* for different intersection angles.

4. The effect of the length of the wedge edges. We checked its effects on the symmetry-breaking instability and the flow structures in the vortical flow regime. We examined whether the unique vortex at the outlet can exist stably as its size increases with increasing length of the wedge, or whether multiple stationary vortices would form and persist in a long wedge.

5. The effect of the outer boundary condition. It is clear that the size of the outer container and the outer boundary condition on the sides of the container can affect substantially the flow outside the wedge. However, it is unclear whether they would affect the

flow inside the wedge significantly. We examined whether the inner flow structures would change substantially when the fluids flow out of the container through the entire downstream side rather than through two slits on the upstream side.

2 Numerical model

2.1 Flow model

The schematic diagram of the flow problem considered is plotted in Fig. 1. We considered only a 2D flow since the flow in the experiment of Putkaradze and Vorobieff (2006) was observed to be 2D. The fluid flows into a wedge-shaped channel through a slit and out of the container through two other slits on the top left and bottom corners of the container. We let the widths of all three slits be equal to each other and be denoted by L_0. The container is set to be square-shaped. We denoted the edge length of the container, the length of the inclined plates (actually the edge length of the wedge) and the intersection angle of the plates as W, L, and α, respectively. Throughout the study, the thickness of the plates was fixed to be $0.5L_0$, as its effect on the flow is expected to be insignificant. The problem specified above resembles the experimental problem of Putkaradze and Vorobieff (2006).

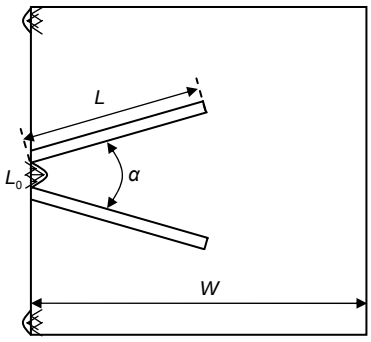

Fig. 1 Schematic diagram of the flow problem considered

The no-slip boundary condition was imposed on all solid walls. The parabolic velocity profile was imposed on both inlet and outlet slits. The average velocity at the inlet was U_0. Since the increase or decrease in the flow flux was considered in the experiment of Putkaradze and Vorobieff (2006), we originally let the flow flux increase or decrease linearly from t=0 to t=t_0 and then remain constant. However, we found that the effect of t_0 on the flow evolution is unimportant, in the sense that the flow evolution is simply more retarded for a larger t_0 and there is no effect of t_0 on flow at steady state (if existing). Hence, we simply let the flow be started suddenly from zero velocity (in the case of increasing flux) or from the velocity at a higher Reynolds number (in the case of decreasing flux).

We took the average velocity U_0 and the width of the slit L_0 as the characteristic velocity and length, respectively. As in the experiment of Putkaradze and Vorobieff (2006), the Reynolds number was defined by

$$Re=\frac{U_0L_0}{\nu}, \tag{1}$$

where ν is the kinematic viscosity of the fluid.

The dimensionless governing equations were

$$\frac{\partial \boldsymbol{u}}{\partial t}+\boldsymbol{u}\cdot\nabla\boldsymbol{u}=\frac{\nabla^2\boldsymbol{u}}{Re}-\nabla p, \tag{2}$$

$$\nabla\cdot\boldsymbol{u}=0, \tag{3}$$

where $\boldsymbol{u}$ and p are the fluid velocity and pressure, respectively.

2.2 Numerical method

The presence of two inclined plates in the square container renders the computation somewhat involved if one employs the conventional methods based on a boundary-fitted mesh. Here, we adopted the direct-forcing fictitious domain (FD) method recently proposed by Yu and Shao (2007). The basis of the method is that the fluid equations Eqs. (2) and (3) are extended into the inner solid domains (plate domains) by introducing a pseudo body-force into the momentum equation Eq. (2) to enforce the no-slip condition on the immersed boundaries (plate edges). Thus, the flow problem can be posed on a larger and simpler domain (a square container). The pseudo body-force can be interpreted as a distributed Lagrange multiplier (Glowinski *et al.*, 1999; 2001). A finite-difference projection method on a homogeneous half-staggered gird was used to solve the flow fields (Yu *et al.*, 2006a; 2006b). For a homogeneous grid, the pressure Poisson equation can be solved efficiently with a fast Fourier transform (FFT)-based solver. All spatial derivatives including

the convective terms were discretized using the second-order central difference scheme (please referred to Yu and Shao (2007) for the details of this method). The FD method has been widely applied to the simulation of particulate flows (Pan *et al.*, 2005; 2007; 2008; Hwang and Hulsen, 2006; Veeramani *et al.*, 2007; Shao *et al.*, 2008). In addition, the commercial Computational Fluid Dynamics (CFD) software FLUENT was employed to validate our computations with the FD code, and to determine the critical Reynolds number for the symmetry-breaking instability.

Owing to the use of the structured mesh that is symmetrical about the centerline of the container, it will take a long (and uncertain) time for the symmetry-breaking instability to take place for a completely symmetrical flow, since the unsymmetrical disturbance is only from the computational round-off error. Therefore, we shifted the center-point of the inlet $0.01L_0$ upwards from the centerline of the container as a small disturbance, to accelerate the possible symmetry-breaking instability.

All results in the present study are given in dimensionless form and obtained with the mesh-size of h=1/8 (i.e., dimensionally $h=L_0/8$) and the time-step of Δt=0.05 (i.e., dimensionally $\Delta t=0.05L_0/U_0$) for our FD computations. We made the mesh-size and time-step convergence checks for a typical case and observed that a further decrease in the mesh-size or time-step results in negligible effects on the results. The accuracy will also be validated by comparison to the FLUENT results.

The convergence criterion for the steady state was

$$\frac{\|\boldsymbol{u}(x,t)-\boldsymbol{u}(x,t-1)\|}{\|\boldsymbol{u}(x,t)\|}<\varepsilon. \tag{4}$$

3 Results and discussion

3.1 Effects of *Re*

We first examine the effects of the Reynolds number on the flow patterns in the wedge for (α, L/L_0, W/L_0)=(32°, 30, 64). Fig. 2 shows the x-component velocity contours and the flow fields at different Re for (α, L/L_0, W/L_0)=(32°, 30, 64). The flow fields in the entire container have satisfied the convergence criterion $\varepsilon=10^{-4}$ for Re<100 (Figs. 2a–2c) by the time indicated in the figure. We find that the flow is symmetrical at Re=30 and becomes unsymmetrical at Re=40. For the unsymmetrical flow, we found that there always exists a backflow, though it may be very weak, which is consistent with the unsymmetrical Jeffery-Hamel solution (Fraenkel, 1962). For all velocity contours in the present study, the interval is 0.1, with one level at −0.05. The maximum velocity of the backflow at Re=40 is smaller than 0.05 and so is not shown in Fig. 2b. The non-symmetry and the backflow are enhanced as Re increases. The backflow is clear for Re=50 in Fig. 2c, though it is still weak. With a further increase in Re, the backflow becomes as strong as the outflow and a vortex appears. Fig. 2d shows such a flow at Re=100. By the simulation time t=5000, the flow has not yet satisfied the steady-state convergence criterion $\varepsilon=10^{-4}$ in Eq. (4), however, we observed that the flow in the wedge changes little from t=2000 to t=5000, indicating that the vortex is stable. From Figs. 2e and 2f, the vortex remains stable at Re=150 (actually also at Re=170 in our simulation), but disappears at Re=180 (also at Re=175), in which case the jet flow in the wedge becomes unsteady. Fig. 3 shows the vorticity contours at Re=200 at t=400 and 500. One can see that the jet attached to one side of the wedge constantly loses stability and rolls up into the mushroom-shaped vortex-pair near the outlet of the wedge where the jet is subject to strong disturbances from the vortices outside the wedge and those shedding from the upper wedge tip.

From the above observations, we can conclude that the flow in the wedge for (α, L/L_0, W/L_0)=(32°, 30, 64) undergoes a change from symmetrical flow (Fig. 2a), to unsymmetrical flow with a weak backflow (Figs. 2b and 2c), then stable vortical (i.e., strong circulation) flow (Figs. 2d and 2e) and finally the unsteady jet flow (Fig. 2f and Fig. 3) as Re is increased. Note that there is no essential difference between the second (the unsymmetrical flow with a weak backflow) and third (the stable vortical flow) regimes since the vortical flow is just an unsymmetrical flow with a strong backflow. We distinguish them only because the flows in Fig. 2b and Fig. 2d appear different.

3.2 Effects of initial condition

As mentioned in Section 1, Putkaradze and Vorobieff (2006) claimed that the critical Reynolds

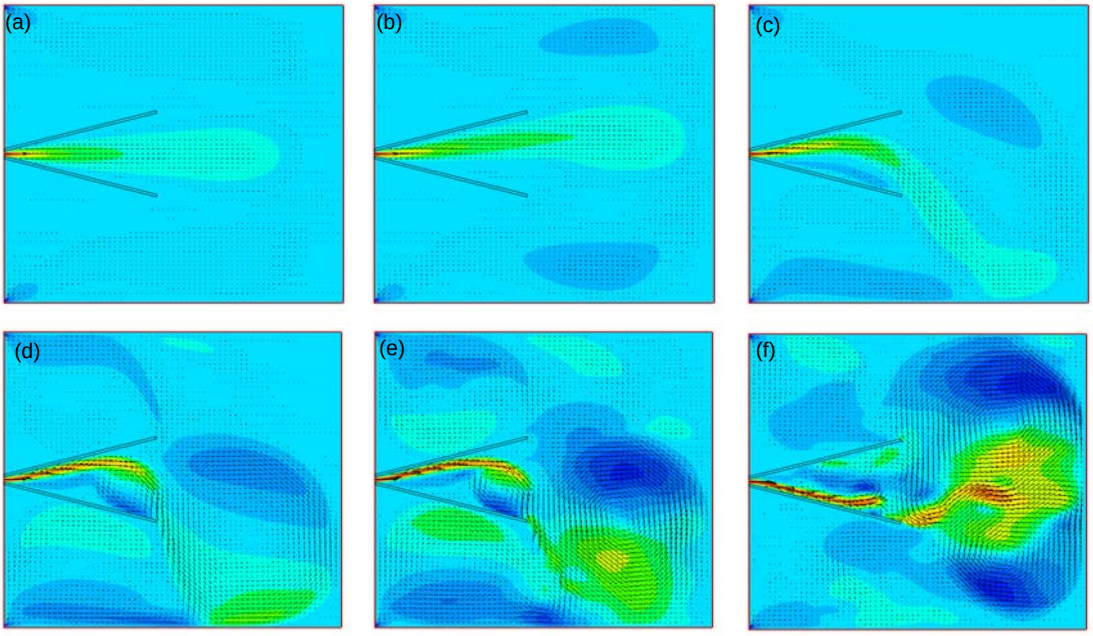

Fig. 2 The *x*-component velocity contours and the flow fields at different *Re* for (α, L/L_0, W/L_0)=(32°, 30, 64).
The entire flows have satisfied the convergence criterion $\varepsilon=10^{-4}$ for (a)-(c) by the time indicated, and the flows in the wedge are stable for (d)–(e) and unstable for (f). For all velocity contours in the present study, the interval is 0.1, with one level at −0.05. (a) *Re*=30, *t*=1550; (b) *Re*=40, *t*=3420; (c) *Re*=50, *t*=3000; (d) *Re*=100, *t*=5000; (e) *Re*=150, *t*=3000; (f) *Re*=180, *t*=3000

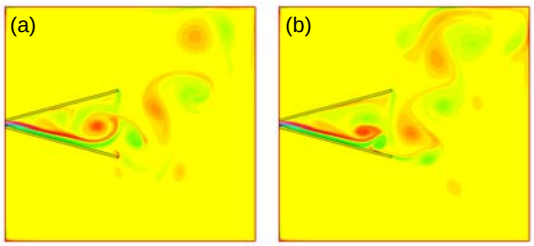

Fig. 3 The vorticity contours for (*Re*, α, L/L_0, W/L_0)=(200, 32°, 30, 64). (a) *t*=400; (b) *t*=500

number for the transition from the symmetrical regime to the vortex regime by increasing the flow flux (referred to as Re_{ci}) was larger than that of the reverse transition caused by decreasing the flow flux (Re_{cd}). They observed two different solutions for a Reynolds number between Re_{ci} and Re_{cd}, depending on whether the flow flux is increased or decreased: an unsteady quasi-symmetrical flow for increasing flux and a steady unsymmetrical flow for decreasing flux. We simulate the flow for *Re*=36 and (α, L/L_0, W/L_0)=(32°, 30, 64) by starting suddenly from zero velocity (increase case) and the velocity at *Re*=40 (decrease case), respectively. The (*x*-component) velocity profiles at *x*=20 and at different times for both cases are plotted in Fig. 4. The evolution of the flow fields at *Re*=36 is found to be very slow. For the increase case, we present the results at *t*=1715, 3225,

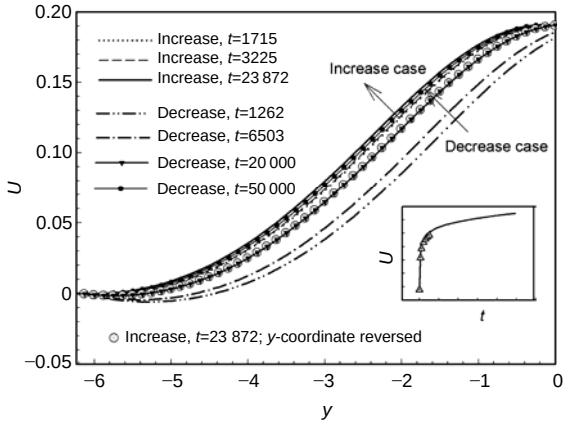

Fig. 4 Time evolutions of the velocity profiles at *x*=20 and *Re*=36 for starting suddenly from zero velocity (increase case) and from *Re*=40 (decrease case). The insert (solid line) shows the time evolutions of the *x*-component velocity from *t*=0 to *t*=50000 at (*x*, *y*)=(20, −2) for the decrease case, and the open triangles represent the FLUENT results

and 23872, the time when the flow satisfies the convergence criteria $\varepsilon=10^{-4}$, 10^{-5} and 10^{-6}, respectively. For the decrease case, the flow meets the convergence criteria $\varepsilon=10^{-4}$ and 10^{-5} at t=1262 and 6503, respectively, but still has not satisfied the condition $\varepsilon=10^{-6}$ by t=50000. The solution for the increase case at t=23872 can be regarded as the steady-state solution, since it is in very good agreement with the steady-state FLUENT results obtained using the dense mesh (Fig. 5b). The velocity profile at t=23872 with the y-coordinate reversed (taking y to be $-y$) also represents the steady-state solution and is plotted in Fig. 4. The solution for the decrease case crosses this steady-state solution around t=20000 and then approaches the other branch of the steady-state solution (Fig. 4). It is surprising that the flow cannot be maintained stably at around t=20000, considering that the local time rate of change of the velocity (i.e., unsteady term) is very small. This may indicate that the flow is not very stable to the disturbance.

Our results do not indicate the presence of two solutions as in the experiments, but could provide a possible and reasonable explanation for the experimental observations. From the definition of the Reynolds number Eq. (1), one can deduce that one dimensionless time unit corresponds to the dimensional one of $t_0=L_0^2/(\nu Re)$. For the experiments, the width of the inlet slit L_0 is 0.2 cm, and the kinematic viscosity of water ν is normally 0.01 cm^2/s, so that $t_0=4/Re$ s, which means that for Re=36, the dimensionless time of 540 amounts to 1 min, and 32400 to 1 h in the experiment. From our simulations, the time for the establishment of the steady solution is at least more than half an hour. In the experiments, disturbance to the flow always exists (owing to the difficulty in keeping the flux constant, unlike in the simulation), which may prolong the unsteady process. In the case of decreasing flux, the flow changes rapidly in the initial stage and then evolves slowly (as shown in the insert of Fig. 4). This could create the false impression that the flow has achieved the steady state just after the initial rapid-development stage and then that there exist two different solutions at the same Reynolds number. In our numerical simulations, one may observe two different (false) steady-state solutions if the criteria $\varepsilon=10^{-4}$ or 10^{-5} are used to judge the convergence (Fig. 4). However, we must stress that our simulations cannot determine what exactly took place in the experiment owing to the differences between our model and the experimental prototype, and therefore cannot exclude the possibility that there were other underlying physics for the hysteresis observed in the experiment. Here, we aim only to examine whether the hysteresis takes place in our flow model and attempt to provide a possible explanation for the hysteresis observed in the experiment.

The commercial CFD software FLUENT is employed to validate our computations with the in-house FD code. The dense mesh with 120352 nodes is adopted for the FLUENT computations. Although the total number of the nodes is still less than that in our FD case (512×512 for W/L_0=64), the grid is much denser in the vicinity of the inlet and the

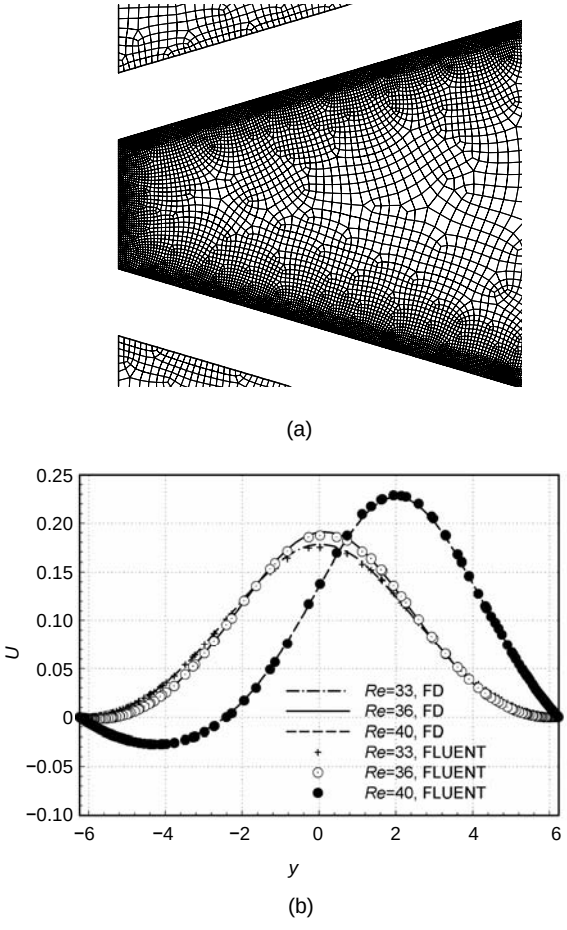

Fig. 5 (a) Mesh for FLUENT computations and (b) comparison between the steady-state velocity profiles at x=20 obtained from the FLUENT and FD computations

wedge wall (Fig. 5a). Steady-state velocity profiles at x=20 for Re=33, 36 and 40 are compared in Fig. 5, and we find good agreement between the two sets of results, in particular near the wedge walls where the dense mesh is used in FLUENT. For the FD results, $\varepsilon=10^{-6}$, and for the FLUENT results, the steady-state criterion is that both velocity and continuity residuals are smaller than 10^{-6}. Because the unsteady computation with FLUENT is very time-consuming, the computation is run only for the case of decreasing flux up to t=5000. The results on the time evolutions of the x-component velocity at (x, y)=(20, −2) are compared to the FD results in the insert of Fig. 4, and good agreement between them can be seen.

3.3 Effects of wedge geometry

We now investigate the effects of the intersection angle and length of the wedge edges on the flow. Putkaradze and Vorobieff (2006) examined the effects of the intersection angle on the critical Reynolds numbers for the transition between the symmetrical and vortical flows at L/L_0=51. We compare our FLUENT results on the critical Reynolds numbers for the symmetry-breaking instability at both L/L_0=30 (W/L_0=64) and L/L_0=51 (W/L_0=128) for α=20°, 32° and 50° to the results of Putkaradze and Vorobieff (2006) and the results from the temporal stability analysis of the Jeffery-Hamel flow (Sobey and Drazin, 1986) in Fig. 6. We determine the critical Reynolds number by checking if there is any negative value in the velocity profile in the wedge at x=20 for L/L_0=30 and x=34 for L/L_0=51. Note that both numerical and experimental data do not represent the exact critical Reynolds numbers but the average values for an interval in which the critical Reynolds numbers fall. The interval for our Re_c is 0.5. For example, in the case of α=32° and L/L_0=30, we find that there is no negative value in the velocity profile at Re=33 and that the negative velocity of (-10^{-5}) occurs in the vicinity of one side wall at Re=33.5, so that Re_c falls in the interval (33.25±0.25). From Fig. 6, analytical, numerical and experimental results all reveal that the critical Reynolds number decreases with increasing intersection angle. The critical Reynolds numbers obtained from the stability analysis, our FLUENT computations, and the experiments in case of decreasing flux agree with each other, which is consistent with our conjecture that the presence of two experimental critical Reynolds numbers is possibly the result of the very slow evolution of the flow at a certain Re regime just above the symmetry-breaking critical Reynolds number. Fig. 6 shows that the effect of the length of the wedge edge on the symmetry-breaking instability is not significant and the critical Reynolds number is slightly smaller for a larger L/L_0.

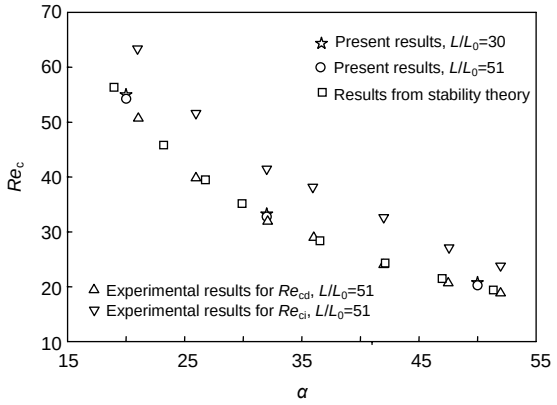

Fig. 6 Comparison between the critical Reynolds numbers for the symmetry-breaking instability obtained from the stability analysis (Sobey and Drazin, 1986) and the FLUENT computations, and the experimental ones for the transition between the symmetrical and vortical flows

The x-component velocity contours and the flow fields at Re=25, 70, 80 and 100 for (α, L/L_0, W/L_0)=(50°, 30, 64) are shown in Fig. 7. For α=32°, we have seen that the flow in the wedge undergoes the change from symmetrical flow, to unsymmetrical flow with a weak backflow, then to vortical flow and finally to an unsteady jet flow as Re is increased. Figs. 7a, 7b and 7d correspond to the latter three flows for α=50°, respectively. The intersection angle has a negative effect not only on the symmetry-breaking instability, but also on the jet instability since the flow becomes unsteady at Re=100 for α=50° (Fig. 7d), whereas the vortex remains stable at Re=150 for α=32° (Fig. 2e). In addition, a new flow pattern between the vortex and unsteady regimes is observed for α=50°: a stable jet attached to one side of the wedge, as shown in Fig.7c. We did not observe this pattern for α=32° where we observed the vortex at Re=170 and the unsteady jet flow at Re=175. The probable reason for the lack of the stable jet flow at α=32° is that the vortex is much more stable at this

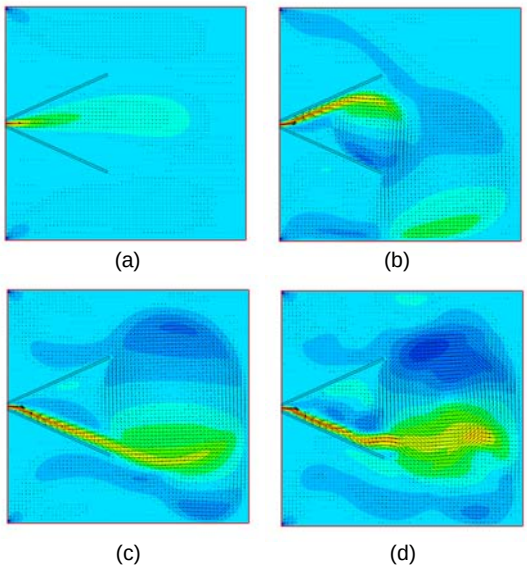

Fig. 7 The *x*-component velocity contours and the flow fields at different *Re* for (α, L/L_0, W/L_0)=(50°, 30, 64). (a) *Re*=25, *t*=3000; (b) *Re*=70, *t*=4100; (c) *Re*=80, *t*=5000; (d) *Re*=100, *t*=5000

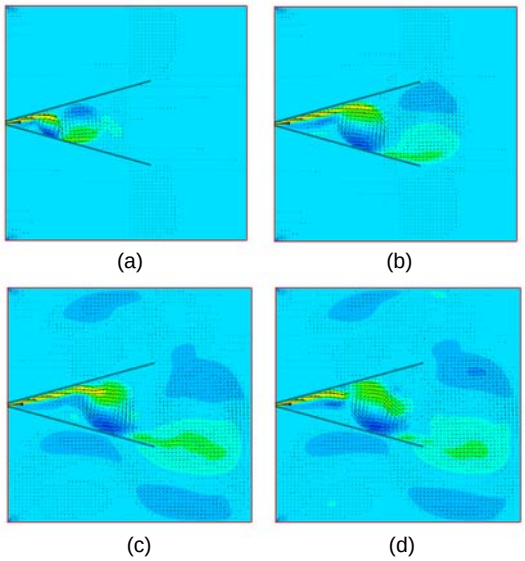

Fig. 8 The *x*-component velocity contours and the flow fields for (*Re*, α, L/L_0, W/L_0)=(100, 32°, 80, 128). (a) *t*=500; (b) *t*=2000; (c) *t*=7000; (d) *t*=7200

smaller value of α and would not lose stability unless *Re* is high enough to cause unsteady jet flow.

It has been shown that a symmetrical flow loses stability slightly more easily with a longer wedge channel (with respect to the slit width L_0). We now examine the effect of the wedge length on the stability of the vortical flow at (*Re*, α)=(100, 32°). For L/L_0=30, the vortex is located at the outlet of the wedge. One may wonder whether multiple vortices would form and exist stably in a longer wedge, as in the simulations of Tutty (1998) and Kerswell *et al.* (2004) for a special expanding channel, or whether the unique vortex at the outlet can exist stably as its size increases with increasing length of the wedge. To answer these two questions, we performed the simulations for (L/L_0, W/L_0)=(80, 128). From Fig. 8, a pair of vortices has appeared by *t*=500, and the outer vortex near the outlet is gradually squeezed out as the inner vortex moves towards the outlet, as observed in the experiment of Putkaradze and Vorobieff (2006). Our results show that there are no multiple stable vortices, and that the unique large vortex exists inside the wedge but is not as stable and close to the outlet as for L/L_0=30 (Figs. 2 and 8). We observe that the jet constantly rolls up into a weak vortex-pair in the vicinity of the large vortex and subsequently they merge into a large vortex. The flow is unsteady. Thus, we can say that both the intersection angle and the wedge length always have negative effects on the stability of the flow in the wedge channel.

To check whether multiple steady vortices would exist in a longer wedge at a lower Reynolds number, the FLUENT software was employed to perform the simulation for (*Re*, α, L/L_0, W/L_0)=(60, 32°, 200, 300). The grid used has 186 352 nodes. The *x*-component velocity contours at steady state are shown in Fig. 9, and one can see that there is only one large vortex inside the wedge.

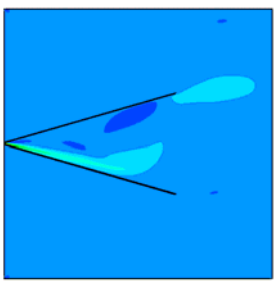

Fig. 9 The *x*-component velocity contours at steady state for (*Re*, α, L/L_0, W/L_0)=(60, 32°, 200, 300), obtained from FLUENT computation

3.4 Effects of outer boundary condition

It is clear that the size of the container and the outer boundary condition on the sides of the container can affect substantially the flow outside the wedge. However, it is unclear whether they would affect the flow in the wedge significantly. To make it clear, we conducted a simulation with the outflow boundary condition imposed on the right side of the container:

$$\frac{\partial \boldsymbol{u}}{\partial t} + u_{\mathrm{a}} \frac{\partial \boldsymbol{u}}{\partial x} = 0,$$

where u_{a} is the average x-component velocity on the boundary, instead of the two small slits on left side of the container. The x-component velocity contours and the flow fields at Re=40 and 100 for the above boundary condition at (α, L/L_0, W/L_0)=(32°, 30, 64) are shown in Fig. 10. The comparison between Fig. 10 and Figs. 2b and 2d indicates that the outer boundary condition does not affect the flow (at least the flow pattern) inside the wedge significantly.

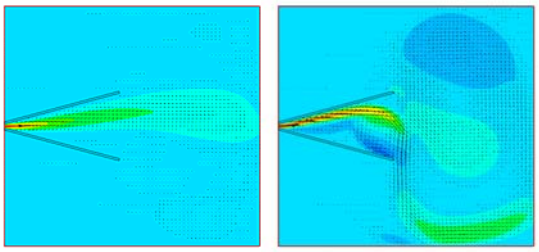

(a) (b)

Fig. 10 The x-component velocity contours and the flow fields at (a) Re=40, t=3040 and (b) Re=100, t=2000 in the case of outflow boundary condition imposed on the right boundary. (α, L/L_0, W/L_0)=(32°, 30, 64)

4 Conclusion

The 2D flow in a wedge-shaped channel opening into a large space was investigated numerically. The following main conclusions can be drawn from the results:

1. At a certain Re regime above the onset of symmetry-breaking instability, the flows evolve into steady state very slowly except for the initial stage in the case of decreasing flow flux. Two different (transient) solutions can be observed within the usual observation time for the experiment, which provides a possible explanation for the hysteresis phenomenon in the experiment.

2. For (α, L/L_0)=(32°, 30), the flow in the wedge undergoes the change from symmetrical flow, to unsymmetrical flow with a weak backflow, then to vortical (circulation) flow and finally to unsteady jet flow as Re is increased. For the unsteady flow, the jet attached to one side of the wedge constantly loses stability and rolls up into the mushroom-shaped vortex-pair near the outlet of the wedge. As α is increased to 50°, a stable jet is observed as a new regime between the vortex and unsteady regimes.

3. Both the intersection angle and the wedge length have negative effects on the stability of the flow, in the sense that the critical Reynolds numbers for the symmetry-breaking instability and the occurrence of the unsteady solution become smaller for a greater intersection angle or wedge length. For (Re, α, L/L_0)=(100, 32°, 80), the vortex inside the wedge is not stable, and the jet constantly rolls up into a weak vortex-pair in the vicinity of the large vortex which subsequently merges into the vortex. In our simulations, the multiple stationary vortices in the wedge are not observed at L/L_0 up to 200.

4. The outer boundary condition does not affect the flow (at least the flow pattern) inside the wedge significantly.

Our numerical results agreed with the experimental observations, but provided a new explanation for the hysteresis phenomenon in the experiment. Some new results were presented to better understand the flow in a finite expanding channel (a classic but not well-understood problem). The accuracy of the fictitious domain method was also validated by comparison to the FLUENT computations with a very fine mesh.

References

Allmen, M.J., Eagles, P.M., 1984. Stability of divergent channel flows: a numerical approach. *Proceedings of the Royal Society A: Mathematical Physical and Engineering Sciences*, **392**(1803):359-372. [doi:10.1098/rspa.1984.0036]

Banks, W.H.H., Drazin, P.G., Zaturska, M.B., 1988. On perturbations of Jeffery-Hamel flow. *Journal of Fluid Mechanics*, **186**:559-581. [doi:10.1017/S0022112088000278]

Boutros, Y.Z., Abd-el-Malek, M.B., Badran, N.A., Hassan, H.S., 2007. Lie-group method solution for

two-dimensional viscous flow between slowly expanding or contracting walls with weak permeability. *Applied Mathematical Modelling*, **31**(6):1092-1108. [doi:10.1016/j.apm.2006.03.026]

Burde, G.I., Nasibullayev, I.S., Zhalij, A., 2007. Stability analysis of a class of unsteady nonparallel incompressible flows via separation of variables. *Physics of Fluids*, **19**(11):114110. [doi:10.1063/1.2814296]

Dennis, S.C.R., Banks, W.H.H., Drazin, P.G., Zaturska, M.B., 1997. Flow along a diverging channel. *Journal of Fluid Mechanics*, **336**:183-202. [doi:10.1017/S0022112096004648]

Eagles, P.M., 1988. Jeffery-Hamel boundary-layer flows over curved beds. *Journal of Fluid Mechanics*, **186**:583-597. [doi:10.1017/S002211208800028X]

Fraenkel, L.E., 1962. Laminar flow in symmetrical channels with slightly curved walls. I. On the Jeffery-Hamel solutions for flow between plane walls. *Proceedings of the Royal Society London A*, **267**:119-138.

Georgiou, G.A., Eagles, P.M., 1985. The stability of flows in channels with small wall curvature. *Journal of Fluid Mechanics*, **159**:259-287. [doi:10.1017/S0022112085003202]

Glowinski, R., Pan, T.W., Hesla, T.I., Joseph, D.D., 1999. A distributed Lagrange multiplier/fictitious domain method for particulate flows. *International Journal of Multiphase Flow*, **25**(5):755-794. [doi:10.1016/S0301-9322(98)00048-2]

Glowinski, R., Pan, T.W., Hesla, T.I., Joseph, D.D., Periaux, J., 2001. A fictitious domain approach to the direct numerical simulation of incompressible viscous flow past moving rigid bodies: Application to particulate flow. *Journal of Computational Physics*, **169**(2):363-426. [doi:10.1006/jcph.2000.6542]

Goldshtik, M., Hussain, F., Shtern, V., 1991. Symmetry breaking in vortex-source and Jeffery-Hamel flows. *Journal of Fluid Mechanics*, **232**:521-566. [doi:10.1017/S0022112091003798]

Hamadiche, M., Scott, J., Jeandel, D., 1994. Temporal stability of Jeffery-Hamel flow. *Journal of Fluid Mechanics*, **268**:71-88. [doi:10.1017/S0022112094001266]

Hamel, G., 1916. Spiralförmige Bewegungen zäher Flüssigkeiten. Jahrber. *Deutsch. Math. Ver.*, **25**:34-60.

Hooper, A.P., Duffy, B.R., Moffatt, H.K., 1982. Flow of fluid of non-uniform viscosity in converging and diverging channels. *Journal of Fluid Mechanics*, **117**:283-304. [doi:10.1017/S0022112082001633]

Hwang, W.R., Hulsen, M.A., 2006. Direct numerical simulations of hard particle suspensions in planar elongational flow. *Journal of Non-Newtonian Fluid Mechanics*, **136**(2-3):167-178. [doi:10.1016/j.jnnfm.2006.04.004]

Jeffery, G.B., 1915. The two-dimensional steady motion of a viscous fluid. *Philosophical Magazine Series 6*, **29**:455.

Kerswell, R.R., Tutty, O.R., Drazin, P.G., 2004. Steady nonlinear waves in diverging channel flow. *Journal of Fluid Mechanics*, **501**:231-250. [doi:10.1017/S0022112003007572]

Landau, L.D., Lifshitz, E.M., 1987. Fluid Mechanics. Pergamon Press, Oxford.

Majdalani, J., Zhou, C., 2003. Moderate-to-large injection and suction driven channel flows with expanding or contracting walls. *ZAMM*, **83**(3):181-196. [doi:10.1002/zamm.200310018]

McAlpine, A., Drazin, P.G., 1998. On the spatio-temporal development of small perturbations of Jeffery-Hamel flows. *Fluid Dynamics Research*, **22**(3):123-138. [doi:10.1016/S0169-5983(97)00049-X]

Nakayama, Y. (Ed.), 1988. Visualized Flow. Pergamon Press, Oxford.

Pan, T.W., Glowinski, Joseph, D.D., 2005. Simulating the dynamics of fluid-cylinder interactions. *Journal of Zhejiang University SCIENCE A*, **6**:97-109. [doi:10.1631/jzus.2005.A0097]

Pan, T.W., Glowinski, R., Hou, S.C., 2007. Direct numerical simulation of pattern formation in a rotating suspension of non-Brownian settling particles in a fully filled cylinder. *Computers and Structures*, **85**(11-14):955-969. [doi:10.1016/j.compstruc.2006.11.007]

Pan, T.W., Chang, C.C., Glowinski, R., 2008. On the motion of a neutrally buoyant ellipsoid in a three-dimensional Poiseuille flow. *Computer Methods in Applied Mechanics and Engineering*, **197**(25-28):2198-2209. [doi:10.1016/j.cma.2007.09.006]

Putkaradze, V., Vorobieff, P., 2006. Instabilities, bifurcations, and multiple solutions in expanding channel flows. *Physical Review Letters*, **97**(14):144502. [doi:10.1103/PhysRevLett.97.144502]

Schlichting, H., Gersten, K., 2000. Boundary Layer Theory (8th Ed.). Springer.

Shao, X., Yu, Z., Sun, B., 2008. Inertial migration of spherical particles in circular Poiseuille flow at moderately high Reynolds numbers. *Physics of Fluids*, **20**(10):103307. [doi:10.1063/1.3005427]

Sobey, I.J., Drazin, P.G., 1986. Bifurcations of two-dimensional channel flows. *Journal of Fluid Mechanics*, **171**:263-287. [doi:10.1017/S0022112086001441]

Stow, S.R., Duck, P.W., Hewitt, R.E., 2001. Three-dimensional extensions to Jeffery-Hamel flow. *Fluid Dynamics Research*, **29**(1):25-46. [doi:10.1016/S0169-5983(01)00017-X]

Tutty, O.R., 1996. Nonlinear development of flow in channels with non-parallel walls. *Journal of Fluid Mechanics*, **326**:263-284. [doi:10.1017/S0022112096008312]

Uribe, F.J., Daz-Herrera, E., Bravo, A., Peralta-Fabi, R., 1997. On the stability of the Jeffery-Hamel flow. *Physics of Fluids*, **9**(9):2798-2800. [doi:10.1063/1.869390]

Veeramani, C., Minev, P.D., Nandakumar, K., 2007. A fictitious domain formulation for flows with rigid particles: A non-Lagrange multiplier version. *Journal of Computational Physics*, **224**(2):867-879. [doi:10.1016/j.jcp.2006.10.028]

Yu, Z., Shao, X., 2007. A direct-forcing fictitious domain method for particulate flows. *Journal of Computational*

Physics, **227**(1):292-314. [doi:10.1016/j.jcp.2007.07.027]

Yu, Z., Shao, X., Wachs, A., 2006a. A fictitious domain method for particulate flows with heat transfer. *Journal of Computational Physics*, **217**(2):424-452. [doi:10.1016/j.jcp.2006.01.016]

Yu, Z., Wachs, A., Peysson, Y., 2006b. Numerical simulation of particle sedimentation in shear-thinning fluids with a fictitious domain method. *Journal of Non-Newtonian Fluid Mechanics*, **136**(2-3):126-139. [doi:10.1016/j.jnnfm.2006.03.015]